ACS APPLIED MATERIALS & INTERFACES

Research Article

www.acsami.org

Phosphorus and Nitrogen Dual-Doped Few-Layered Porous Graphene: A High-Performance Anode Material for Lithium-Ion Batteries

Xinlong Ma,[†] Guoqing Ning,*[,†] Chuanlei Qi, Chenggen Xu, and Jinsen Gao

State Key Laboratory of Heavy Oil Processing, China University of Petroleum, Beijing, Changping 102249, P. R. China

Supporting Information

ABSTRACT: Few-layered graphene networks composed of phosphorus and nitrogen dual-doped porous graphene (PNG) are synthesized via a MgO-templated chemical vapor deposition (CVD) using $(NH_4)_3PO_4$ as N and P source. P and N atoms have been substitutionally doped in graphene networks since the doping takes place at the same time with the graphene growth in the CVD process. Raman spectra show that the amount of defects or disorders increases after P and N atoms are incorporated into graphene frameworks. The doping levels of P and N measured by X-ray photoelectron spectroscopy are 0.6 and 2.6 at %, respectively. As anodes for Li ion batteries (LIBs), the PNG electrode exhibits high reversible capacity (2250 mA h g^{-1} at the current density of 50 mA g^{-1}), excellent rate capability (750 mA h g^{-1} at 1000 mA g^{-1}), and satisfactory cycling stability (no capacity decay after 1500 cycles), showing much enhanced electrode performance as compared to the undoped few-layered porous graphene. Our results show that the PNG is a promising candidate for anode materials in high-rate LIBs.

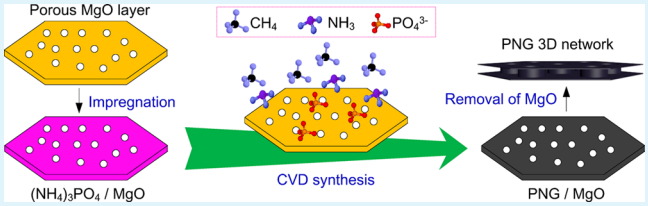

KEYWORDS: *phosphorus doping, porous graphene, chemical vapor deposition, lithium-ion battery, anode*

1. INTRODUCTION

High energy density, long cycle life, as well as high rate performance of lithium-ion batteries (LIBs) are essential for portable electronic devices and powering electric vehicles in the modern society. Graphite, which is widely used as the commercial anode material in LIBs, has excellent cycling stability but low theoretical specific capacity (372 mA h g^{-1}) and poor rate performance.[1] To meet the increasing requirements for LIBs with high capacity and high power density, carbon nanomaterials with high electrical conductivity and well-developed porous structure have been developed to obtain large Li storage capacity and fast Li^+ diffusion.[2−8] On the other hand, heteroatom doping of graphene crystal lattices can tailor both the chemical reactivity and the electronic and physical properties,[9−16] which has been applied to enhance the electrode performance in LIBs.[8,17] For instance, N-doped graphene presents better electrochemical performance as anode in LIBs than the pristine graphene because of the incorporation of N to graphene framework offering more active sites and altering the electronic performance, which is beneficial to Li^+ storage and diffusion during cycling.[18,19] P and N are in the same family, whereas the former has higher electron-donating ability and exhibits stronger n-type behavior.[20] Previous studies have demonstrated that P-doped carbon materials with a small amount of P concentration exhibit excellent electrocatalytic activity, long durability, and high selectivity when they are employed as metal-free catalysts for oxygen reduction reaction (ORR) in fuel cells.[20−22] Choi et al. further confirmed that P, N dual-doped carbon exhibited much higher catalytic activity than the sole N-doped carbon in ORR, indicating that the additional P doping could significantly promote the catalytic activity.[23,24] Similar contribution to the improvement of specific capacitance by P, N codopings or sole P doping for carbon materials is also observed in supercapacitors.[25−27] Futhermore, P, N codoped multiwalled carbon nanotubes (CNTs) have been used as the chemical sensor, exhibiting a higher chemical reactivity as compared to the N-doped CNTs produced under the same experimental conditions.[28] Although the excellent performance of P- and N-doped carbon materials for the applications in fuel cells and supercapacitors have been widely investigated, to our knowledge, the application of P-doped carbon materials in the field of LIBs has not been reported.

The defective graphene contains more defects and exhibits a higher Li storage capacity as compared to the commercial graphite due to the fact that the former can significantly reduce the diffusion resistance and distance between graphene and Li, as well as provides more edges on sheet for the enhancement of Li storage.[5,6] The greatly enhanced capacity in disordered graphene nanosheets was confirmed to be mainly ascribed to additional reversible storage sites such as edges and other defects.[7] Theoretical study also demonstrated that Li^+ could diffuse fast toward the edges due to the lower energy barrier and diffusion length. The presence of these edges affected not only the reactivity of the carbon material toward the adsorption

Received: June 11, 2014
Accepted: August 8, 2014
Published: August 8, 2014

of Li but also their diffusion properties.[29] In addition, doping of graphene with heteroatoms such as N, S, and B is able to introduce defects/disorders into graphene nanosheets and creat a great number of active sites through modulation of the band structure of graphene, which effectively contributes to providing more storage regions, enhancing the electronic conductivity as well as the lithium electroactivity.[8,19,30]

Currently, most N- or P-doped graphenes were synthesized by the thermal reaction of graphene with NH_3, N_2, and N- or P-containing organic compounds at high temperature.[8,19,20,24,31] The distribution of the heteroatoms is not considerable, and additionally, the irreversible stacking of graphene always occurred by the direct thermal annealing process because of the strong π-interactions. Fortunately, the chemical vapor deposition (CVD) process is capable of producing high-quality graphene with few-layered graphene and reducing the stacking degree of graphene.[32,33] Here, a facile one-step CVD approach is developed to synthesize the P and N dual-doped nanomesh graphene (PNG) through an in situ doping process, which is able to guarantee the uniform distribution of heteroatoms. The three-dimensional (3D) PNG network composing of 1−4 graphene layers has P and N concentrations of ∼0.6 and 2.6 at %. Combining the excellent structural design and the uniform heteroatom doping, the PNG exhibits an extraordinary electrochemical performance as anodes in LIBs. The reversible capacity of the PNG is up to 2250 mA h g^{-1} at the current density of 50 mA g^{-1}, about twice the value for the undoped porous graphene. It is concluded that the contribution of P doping to the electrochemical performance of graphene is superior to N doping. Our results indicate that P doping can efficiently promote the Li storage capacity, and that the as-synthesized PNG is a reliable anode material with high energy and power density.

2. EXPERIMENTAL SECTION

First, purchased MgO powder (Sinopharm Chemical Reagent Co. Ltd.) was mixed with deionized water accompanied by ultrasonic agitation. The mixture was boiled for 24 h in a reflux apparatus. After filtration and drying, the material obtained was ground into a fine powder. Porous MgO layers were obtained after calcined at 500 °C for 30 min to remove water. Then, the porous MgO layers were ultrasonically dispersed in $(NH_4)_3PO_4$ solution for 1 h. The as-obtained suspension was dried in a vacuum oven at 80 °C for 24 h to get a white solid mixture. Then the mixture was fed into a vertical quartz reactor from the top hopper after the reaction temperature reaches 900 °C in an argon flow, and CH_4 was introduced into the reactor and maintained for 10 min. After cooling to room temperature, the as-obtained black powder was taken out and purified by excessive amount of hydrochloric acid to obtain the final product. For comparison, using pure MgO layers as templates, undoped porous graphene (labeled as G) was synthesized by CH_4 cracking, and a N-doped graphene-CNT composite (labeled as NG) was obtained by introducing NH_3 into the reactant gas. P-doped graphene (labeled as PG) was synthesized using $Mg_3(PO_4)_2$ as templates and CH_4 as carbon source.

The as-prepared carbon materials were characterized by scanning electron microscope (SEM, Quanta 200F), transmission electron microscope (TEM, F20), X-ray diffraction (XRD, Bruker D8 Advance), Brunauer−Emmett−Teller surface area measurements (BET, Micromeritics ASAP 2020), Raman spectrometer (Renishaw RM2000) with the 633 nm wavelength and X-ray photoelectron spectroscopy (XPS, PHI700). $(NH_4)_3PO_4{\cdot}3H_2O$ was characterized by Thermogravimetric analysis (TGA, NETZSCH STA409PC).

Typically, 70 wt % graphene material, 10 wt % acetylene black and 20 wt % polyvinylidene fluoride were mixed in *N*-methyl-2-pyrrolidinone to obtain a slurry. The slurry was spread onto a copper foil and then dried in a vacuum oven at 105 °C for 24 h to remove solvent. After pressed at 2 MPa, the foil was cut into disks (13 mm in diameter) and dried at 110 °C for 12 h in vacuum. The loading of graphene materials is ∼1 mg for each electrode. Coin-type cells of 2025 were assembled in an Ar-filled glovebox. The electrolyte was synthesized by 1 M $LiPF_6$ dissolved in a mixed solvent of ethylene and dimethyl carbonate with a volume ratio of 1:1, and lithium metal foil was used as the counter/reference electrode. The charge and discharge were conducted on a battery test system at 25 °C at the current densities from 50 to 1000 mA g^{-1} between 0.01 and 3 V vs Li^+/Li at room temperature. Cyclic voltammetry (CV) measurements were carried out on an electrochemical workstation (CHI660D) at a scan rate of 0.1 mV s^{-1}. Electrochemical impedance spectrum measurements were carried out on CHI660D with frequency range of 0.1 Hz to 100 kHz. The current−voltage (I−V) curves were obtained on CHI660D using the compressed pellets (100 mg) of 13 mm in diameter, which are pressed in a stainless steel mold by using 10 MPa pressure.

3. RESULTS AND DISCUSSION

The synthetic strategy for PNG is illustrated in Figure 1. $(NH_4)_3PO_4$/MgO composite layers prepared by an impregnation method are used as both the templates and the P and N source in the CVD process. CH_4 cracking in the presence of NH_3 and PO_4^{3-} leads to the growth of PNG on the surface of porous MgO layers. 3D networks of PNG with a pillar-supported porous structure are finally obtained after removal of the porous MgO templates. The mass ratios between $(NH_4)_3PO_4$ and MgO are 2:1 and 1:1, corresponding to the products labeled as PNG2 and PNG1. G was synthesized by CH_4 cracking, using pure MgO layers as templates.[32] The SEM images of G, PNG1, and PNG2 are shown in Figure 2, revealing a similar porous morphology. In Figure 3a-c, a highly porous structure with nanopores of 2−10 nm is clearly observed in PNG2. High resolution TEM observation (Figure 3b) shows that PNG2 composes of 1−4 layered graphene. The few-layer structure of PNG2 is further confirmed by the AFM observation. As shown in Figure 4, the thickness of the graphene sheets measured by AFM is about 0.8 nm, indicating that it contains no more than two graphene layers. The existence of nanopores in the graphene sheet can be clearly observed in the height profiles, as indicated by the arrows. Further TEM observation (see Figure S1 in the Supporting Information) shows that the morphology of G is similar to PNG2. Agglomeration of the graphene sheets is avoided due to the obvious surface corrugations and the 3D pillar-supported structure, as previously reported.[32] Therefore, a specific surface area (SSA) as high as 1840 m^2 g^{-1} is obtained for PNG2. Energy-dispersive spectrometer (EDS) elemental mapping of PNG2 indicates that C, P, and N are uniformly distributed throughout the whole area (Figure 3d).

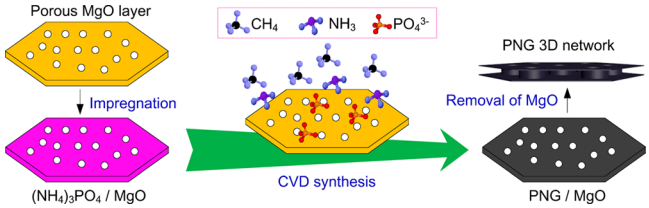

Figure 1. Schematic Illustration of the Fabrication of PNG.

In our lab, both few-layered and multilayered porous graphene have been prepared by using CH_4 and C_2H_4 as carbon source, respectively. The few-layered graphene derived

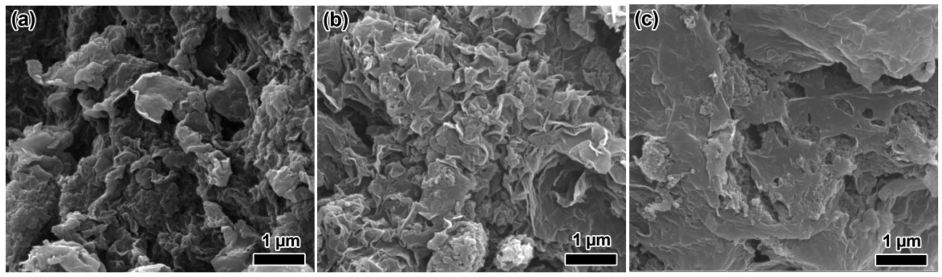

Figure 2. SEM images of (a) G, (b) PNG1, and (c) PNG2.

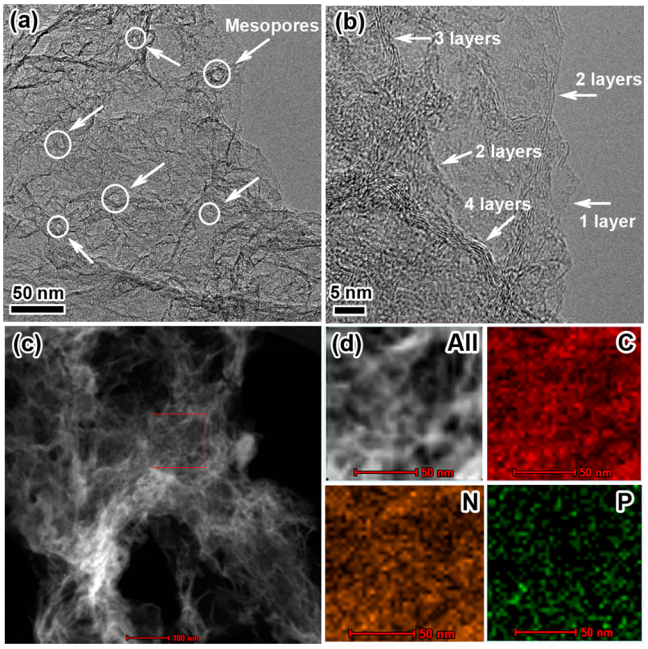

Figure 3. (a, b) Transmission electron microscope (TEM), (c) scanning transmission electron microscope (STEM) images, and (d) EDS elemental mapping of PNG2.

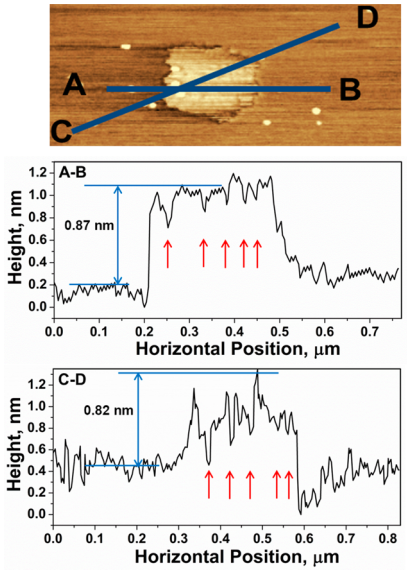

Figure 4. AFM image and height profiles of PNG2. The arrows in the height profiles indicate the existence of pores in the graphene sheet.

by CH_4 cracking is more flexible as compared to the multilayered graphene derived by C_2H_4 cracking. It is difficult to clearly observe a single graphene sheet for the few-layered graphene because of deformation and tangling of the flexible sheets. Fortunately, the pillar-supported porous structure can be easily observed in the multilayered graphene sheets, as shown in Figure S2 in the Supporting Information. Rigid flakes can be observed in SEM observation (see Figure S2a in the Supporting Information), quite different with the appearance of the few-layered graphene sheets (Figure 2). The pillar-supported 3D networks illustrated in Figure 1 can be clearly observed in the electron microscope observations of the multilayered graphene (see Figure S2 in the Supporting Information). Because of the similar formation mechanism, it is reasonable to consider that the few-layered graphene sheet also have such a pillar-supported 3D network structure.[34]

XPS analysis was carried out to determine the doping levels and bonding configurations of N and P in PNG nanosheets. As shown in Figure 5a, peaks at ~133 and 400 eV, corresponding to P 2p and N 1s peaks, respectively, are observed for PNG2.[13,22] The existence of O atoms in all porous graphene materials is ascribed to the adsorption of water and oxygen on the surface.[35] The fine split peaks in the high-resolution P 2p spectra (Figure 5b) reveal that P is covalently bonded with C, and exists as tetrahedral forms such as C_3−PO, C_2−PO_2, and C−PO_3 (131.8 and 133.2 eV) that commonly occur in phosphoric acid activated carbons.[26,36] The presence of both P−O bonding (134.2 eV) and P−C bonding (130.6 and 135.0 eV) are also observed in P 2p spectra.[20,22,23,37,38] N 1s XPS spectra (Figure 5c) can be deconvoluted into three different peaks at 398.4, 400.1, and 401.7 eV, corresponding to pyridinic-N, pyrrolic-N and graphitic-N based on references related to N-doped carbon materials.[8,18,39,40] The doping levels of P and N in PNG2 measured by XPS are 0.6 and 2.6 at %, respectively. Smaller P and N concentrations are found in PNG1 and no peaks corresponding to P and N are observed for G, indicating that introduction of $(NH_4)_3PO_4$ has contributed to the P and N doping. Raman spectra of G, PNG1 and PNG2 are shown in Figure 5d. The G band corresponds to the zone center E_{2g} symmetry related to phonon vibrations in sp^2 carbon materials, whereas the high intensity of the D band with A_{1g} symmetry is ascribed to disordered carbon, edge defects, and other defects.[41−44] The intensity ratio of D band to G band (I_D/I_G) represents the disorder degree of graphene. PNG2 occupies the highest value of I_D/I_G (1.83) among them, indicating that more defects or disorders introduced by P and N exist in the edges of PNG2. Compared to the undoped graphene G, the strengthened D bands of PNG1 and PNG2 are ascribed to the doping itself. Because the Raman analysis is not fully elucidating for estimating the graphitization degree of a doped carbon material, XRD analysis was conducted. As

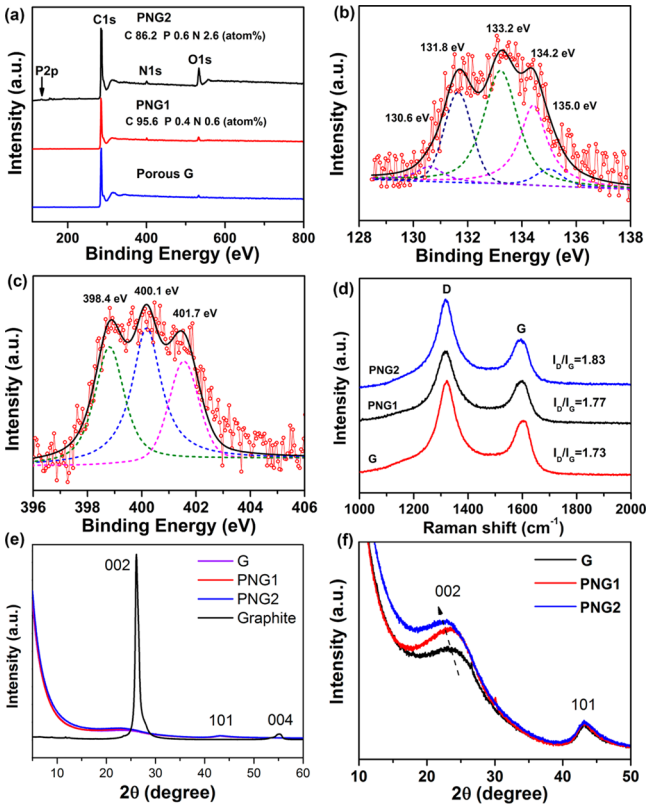

Figure 5. (a) XPS survey spectra of G, PNG1 and PNG2. (b) P 2p and (c) N 1s spectra of PNG2. (d) Raman spectra of G, PNG1, and PNG2. (e) XRD patterns of G, PNG1, and PNG2 in comparison with graphite. (f) Magnified XRD patterns of G, PNG1, and PNG2.

shown in Figure 5e, the 002 peaks for the porous graphene G, PNG1 and PNG2 are centered at 22.9−23.6°, showing an obvious downshift as compared to graphite (26.1°). It means that the interlayer spacing in the few-layered graphene is larger than that in graphite. In the magnified XRD patterns (Figure 5f), a slight downshif of the 002 peak is observed for PNG1 and PNG2 as compared to the undoped graphene (G), implying that the interlayer spacing has been further increased by the P and N dual doping. Compared to graphite, the intensities of the 002 peaks for the porous graphene samples are much lower, indicating that the porous graphene samples have low graphitization degrees. The intensity of the 002 peaks for PNG1 and PNG2 is higher than that for G, showing that PNG1 and PNG2 have higher graphitization degrees as compared to G.

TGA (see Figure S3 in the Supporting Information) shows that $(NH_4)_3PO_4$ will release NH_3 at a temperature higher than 700 °C due to the decomposition of $(NH_4)_3PO_4$. $Mg_3(PO_4)_2$ is first formed due to the reaction between MgO and H_3PO_4 (detected by XRD, see Figure S4 in the Supporting Information). In this reaction system, the C atoms derived by CH_4 cracking recombine with the N atoms from NH_3 and the P atoms from phosphate anion via covalent bonds, thus leading to an in situ P and N dual dopings. When a CH_4 and NH_3 mixture is used as reactant gas and MgO porous layers are used as templates, a N-doped graphene-CNT composite (labeled as NG) is obtained (see Figure S5 in the Supporting Information),[45] forming a sharp contrast to the as-synthesized few-layer graphene layers in PNG2, indicating that the functional group of phosphate can suppress the CNTs growth. The N concentration in NG measured by XPS is 3.9 at %, and the N 1s spectra of NG is similar to that of PNG2 (see Figure S6 ub tge Supporting Information). The amount of NH_3 increases while the amount of $(NH_4)_3PO_4$ increases, thus resulting in a higher N concentration in PNG2 as compared to PNG1. Because only the $Mg_3(PO_4)_2$ exposed on the outside surface could serve as the P source, P concentration does not significantly increase as the amount of $(NH_4)_3PO_4$ increases. Sole P-doped graphene (labeled as PG) was synthesized using $Mg_3(PO_4)_2$ as a template, and its P concentration (0.3 at %) is comparable to that of PNG1 (see Figure S7 in the Supporting Information). PG has a wrinkled morphology (see Figure S8 in the Supporting Information) and few-layered structure similar to PNG2, with an even distribution of P element (see Figure S9 in the Supporting Information). N_2 adsorption−desorption isotherms of type IV with H2-type distinct hysteresis loops and similar pore size distributions centralizing at 2−10 nm are observed for all the as-prepared graphene samples (Figure 6), indicating the graphene samples prepared by the CVD processes have similar porous morphologies. The SSAs of G, PG and PNG1 are 1743, 1748, and1752 $m^2\ g^{-1}$, comparable to that of PNG2 (1840 $m^2\ g^{-1}$). The SSA of NG (1596 $m^2\ g^{-1}$) is

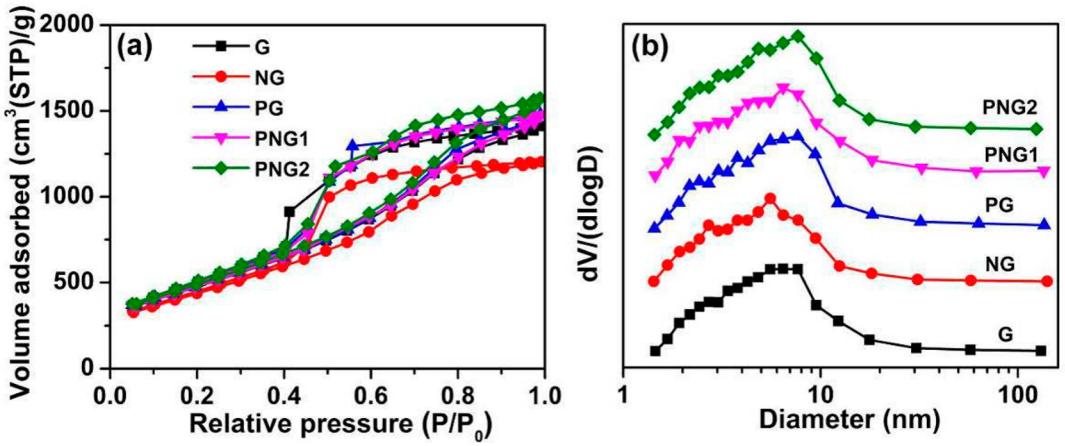

Figure 6. (a) N_2 adsorption/desorption isotherms and (b) pore size distributions of the as-prepared materials. The pore size distribution patterns are calculated from the absorption curves.

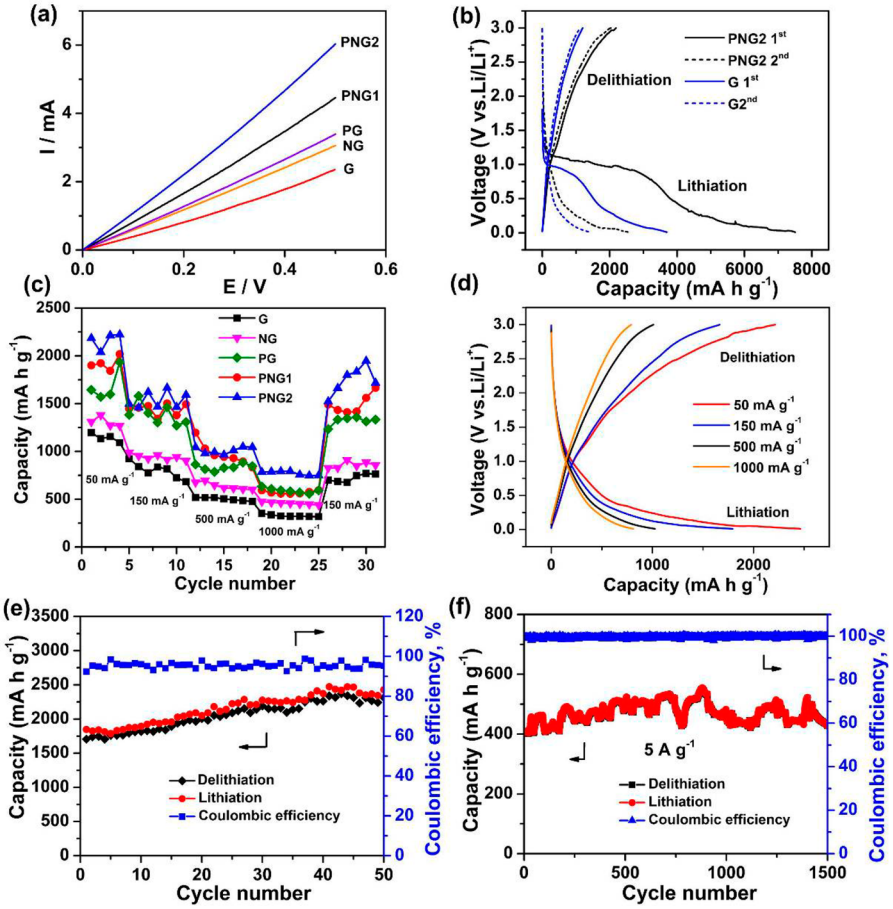

Figure 7. (a) *I*−*V* curves of the as-prepared porous graphene samples. (b) Galvanostatic lithiation/delithiation curves of G and PNG2 electrodes for the 1st and 2nd cycles at the current density of 50 mA g^{-1}. (c) Rate capabilities of G, NG, PG, PNG1, and PNG2 electrodes at different current densities. (d) Typical galvanostatic lithiation/delithiation curves of PNG2 electrode at different current densities. Cycling stability of PNG2 electrode at the current density of (e) 150 mA g^{-1} and (f) 5 A g^{-1}.

slightly lower than the others because of containing some CNTs.

Figure 7a shows the *I*−*V* curves of the tablets containing the as-prepared graphene materials. PNG2 affords the highest charge conductivity among all the samples, follwed by PNG1, and the conductivity of G is the lowest. It indicates that P and N dual doping can significantly promote the electronic conductivity of graphene. PG (with a P concentration of only 0.3 at %) delivers higher conductivity than NG (with a N concentration of 3.6 at %), indicating that the contribution of P to the enhancement of electronic conductivity is higher than that of N. Previously theoretical calculations have demonstrated that P doping is able to improve the electron-donor properties of a carbon material,[46−48] conclusively accompanied by an increased conductivity, which is consistent with our results.

Coin cells were assembled using the as-prepared porous graphene as anode materials. As shown in Figure 7b, PNG2 delivers a lithiation capacity of 7507 mA h g^{-1} and a delithiation capacity of 2185 mA h g^{-1} at the current density of 50 mA g^{-1} in the first cycle, corresponding to a couloumbic efficiency of 30%. In contrast, the initial lithiation capacity and delithiation capacity for the undoped graphene (G) are 3695 and 1197 mA h g^{-1}, respectively, much lower than those for PNG2. A voltage plateau at around 1.0 V is observed in the initial lithiation process for PNG2 and G electrodes, which can be assigned to the decomposition of electrolyte and the formation of the solid electrolyte interphase (SEI) film.[49] Then the large irreversible capacity can be attributed to the formation of SEI films on the highly defective porous graphene with a high SSA.[6,50,51] The initial large irreversible capacity could be decreased efficiently after the electrode material was prelithiated, enhancing the initial couloumbic efficiency (seeFigure S10 in the Supporting Information).[52] It is noticeable that the capacity at 0−0.5 V for PNG2 is 2044 mA h g^{-1} in the second cycle, corresponding to 80% of the total lithiation capacity (2569 mA h g^{-1}). The first cathodic peaks at about 0.4 V were observed for G, PG and PNG2 in the first cycle (see Figure S11 in the Supporting Information), corresponding to the irreversible Li consumption due to formation of SEI films.[53] However, the peak of PNG2 is much weaker than that of G, reflecting that a thinner SEI film can be afforded by it.

The rate capabilities of G, NG, PG, PNG1, and PNG2 at various lithiation/delithiation rates are presented in Figure 7c. The reversible capacity for PG is 1360 mA h g^{-1} at the current density of 150 mA g^{-1} and 580 mA h g^{-1} at 1000 mA g^{-1}, which is 1.9 and 1.8 times that for G, respectively. Because PG and G have similar morphology and structure, the promotion in the reversible capacity for PG should be attributed to the P doping. PNG2 affords the highest capacity among all samples under different current densities, embodying its excellent rate capability. The reversible capacity for PNG2 at the current density of 50 mA g^{-1} is up to 2250 mA h g^{-1}. At the current

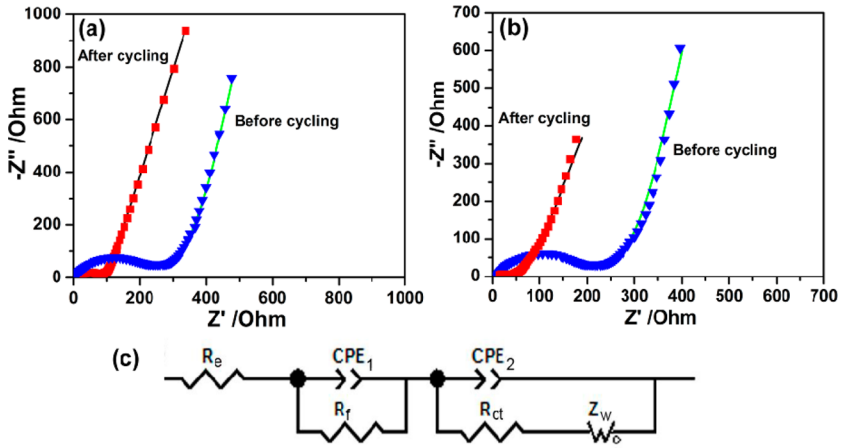

Figure 8. Nyquist plots of (a) G and (b) PNG2. The scatters show the raw data, and the lines show the fitting curves. (c) Equivalent circuit used to fit the experimental data. In the equivalent circuit, R_e represents the total resistance of electrolyte, electrode, and separator. R_f and CPE_1 are the resistance and capacitance (expressed by a constant phase element), respectively, of the SEI formed on the electrode. R_{ct} and CPE_2 represent the charge-transfer resistance and the double layer capacitance, respectively, and Z_w is the Warburg impedance related to the diffusion of lithium ions into the bulk electrode.

density of 1000 mA g^{-1}, the PNG2 electrode delivers a reversible capacity of 750 mA h g^{-1}, which is much higher than the value for the undoped porous graphene G (300 mA h g^{-1}). PNG2 has a N doping level comparable to the sole N doped sample (NG), but exhibits much better rate capability, indicating that the enhanced capacity is mainly contributed by P doping. Although N doping has been reported as an efficient approach to promoting the Li storage capability,[19,54] our results indicate that P doping is more efficient than N doping for this purpose. PG has a rate capability comparable to PNG1, probably because of the same doping level of P. The rate capability for PNG2 is also much better as compared to other graphene or heteroatom-doped graphene materials (e.g., 445 mA h g^{-1} at 1000 mA g^{-1} for graphene sheets,[55] 718 mA h g^{-1} at 500 mA g^{-1} for N-doped graphene[17]). Figure 7d presents the lithiation/delithiation curves of PNG2 without obvious plateaus at different current densities. Previous study has demonstrated that the absence of a potential plateau suggests a disordered stacking of the graphene nanosheet structures, resulting in electrochemically and geometrically nonequivalent lithium ion sites.[5] The contribution of lithium intercalation into the graphene layers to the capacity (below 0.5 V) is 80, 77, 67, and 63% for 50, 150, 500, and 1000 mA g^{-1}, and the rest of capacity is contributed by Faradaic capacitance on the surface or on the edge sites of sheets.[5,6,56] This indicates that the lithiation processes are carried out mainly at the voltage range of 0−0.5 V, which is in favor of obtaining a higher working voltage in a full battery.

The cycling performance of PNG2 at a low current density (150 mA g^{-1}) is shown in Figure 7e. The reversible capacity increases gradually during cycling, which can be acsribed to the gradual activation of porous graphene during the cycling process.[57] An increase of 36% in the reversible capacity (from 1705 to 2313 mA h g^{-1}) is observed for PNG2 after 50 cycles at 150 mA g^{-1}. Similar gradual increase in Li storage capacity is also observed in G, NG, PG, and PNG1 (see Figure S12 in the Supporting Information). Moreover, PNG2 delivers a reversible capacity of 450 mA h g^{-1} with a stable Coulombic efficiency ~100% at the current density of 5 A g^{-1}, and almost no capacity decay is observed after 1500 cycles (Figure 7f andFigure S13 in the Supporting Information), showing an excellent cycling stability.

The reasons of the superior rate capability and cycling stability of PNG2 are proposed. First, the hierarchical 3D porous structure of PNG2 is conducive to absorbing Li^+ and also serves as a reservoir for Li storage. Second, P and N dual doping has induced a large amount of defects on the graphene layer to enhance the interaction property of Li^+, thus enhancing its electrochemical performance.[39] Previous study suggested that substitutional P was incorporated into the structure at the edge-plane sites of the carbonaceous materials due to the larger atomic size (0.106 nm vs 0.077 nm).[58] Therefore, it is conceivable that the substitutional P atoms at the edge-plane sites serve to expand the layer planes, resulting in storing more Li^+,[59] which contributes to the enhancement of the Li^+ uptake. Third, the electrical conductivity is improved significantly after the P and N dual doping. AC impedance analysis (Figure 8 and Table S1 in the Supporting Information) shows that the charge-transfer resistance and SEI resistance of PNG2 (12.9 and 6.9 Ω) are much smaller than those of G (38.7 and 20.5 Ω) after cycling, which are beneficial to fast Li^+ diffusion and quick charge transfer at the interface between the electrolyte and the electrode.

Fluctuation of capacity is observed in Figure 7c, e, and f. During the cycling at 150 mA/g (Figure 7e and Figure S12 in the Supporting Information), the Li storage capacity is gradually increased with fluctuations, which corresponds to the increase and fluctuations in Li storage rooms. Similar fluctuation of capacity is also observed in other porous carbon materials.[6,60] We consider that the capacity fluctuation is related to the pore-confined insertion and extraction of Li ions. Because of the good flexibility of the few-layered porous graphene, the pore structure might gradually change with the cycling, thus leading to changes in pore volume. Further work on this point is still under the way.

4. CONCLUSION

In summary, few-layered graphene networks composing of PNG were synthesized via a MgO-templated chemical vapor deposition using $(NH_4)_3PO_4$ as N and P source. XPS analysis shows that P and N atoms have been substitutionally doped in

graphene networks via covalent bonds. Raman analysis indicates that the amount of defects or disorders increases after the P and N doping. The doping levels of P and N measured by XPS are 0.6 and 2.6 at %, respectively. As anodes in LIBs, the PNG exhibits high reversible capacity (2250 mA h g^{-1} at the current density of 50 mA g^{-1}), excellent rate capability (750 mA h g^{-1} at 1000 mA g^{-1}) and satisfactory cycling stability (no capacity decay after 1500 cycles), showing a significant promotion as compared to the undoped few-layered porous graphene. Compared to N doping, P doping is more efficient to promote the Li storage capacity for graphene materials. Our work reveals that P doping can efficiently enhance the Li storage capacity, and provides a useful strategy to synthesize high-performance anode materials by combining elaborate structure control and the heteroatom doping technique together.

■ ASSOCIATED CONTENT

Supporting Information

Additional figures. This material is available free of charge via the Internet at http://pubs.acs.org/.

■ AUTHOR INFORMATION

Corresponding Author

*E-mail: ngq@cup.edu.cn.

Author Contributions

†Authors X.M. and G.N. contributed equally.

Notes

The authors declare no competing financial interest.

■ ACKNOWLEDGMENTS

This work was supported by the National Natural Science Foundation of China (21206191) and the Science Foundation of China University of Petroleum, Beijing (2462013YXBS007).

■ REFERENCES

(1) Geim, A. K.; Novoselov, K. S. The Rise of Graphene. *Nat. Mater.* **2007**, *6*, 183−191.

(2) Novoselov, K. S.; Geim, A. K.; Morozov, S. V.; Jiang, D.; Zhang, Y.; Dubonos, S. V.; Grigorieva, I. V.; Firsov, A. A. Electric Field Effect in Atomically Thin Carbon Films. *Science* **2004**, *306*, 666−669.

(3) Yu, Y.; Gu, L.; Wang, C.; Dhanabalan, A.; van Aken, P. A.; Maier, J. Encapsulation of Sn@carbon Nanoparticles in Bamboo-like Hollow Carbon Nanofibers as an Anode Material in Lithium-Based Batteries. *Angew. Chem., Int. Ed.* **2009**, *48*, 6485−6489.

(4) Geim, A. K. Graphene: Status and Prospects. *Science* **2009**, *324*, 1530−1534.

(5) Yoo, E.; Kim, J.; Hosono, E.; Zhou, H.-s.; Kudo, T.; Honma, I. Large Reversible Li Storage of Graphene Nanosheet Families for Use in Rechargeable Lithium Ion Batteries. *Nano Lett.* **2008**, *8*, 2277−2282.

(6) Fan, Z.; Yan, J.; Ning, G.; Wei, T.; Zhi, L.; Wei, F. Porous Graphene Networks as High Performance Anode Materials for Lithium Ion Batteries. *Carbon* **2013**, *60*, 558−561.

(7) Pan, D.; Wang, S.; Zhao, B.; Wu, M.; Zhang, H.; Wang, Y.; Jiao, Z. Li Storage Properties of Disordered Graphene Nanosheets. *Chem. Mater.* **2009**, *21*, 3136−3142.

(8) Wu, Z.-S.; Ren, W.; Xu, L.; Li, F.; Cheng, H.-M. Doped Graphene Sheets as Anode Materials with Superhigh Rate and Large Capacity for Lithium Ion Batteries. *ACS Nano* **2011**, *5*, 5463−5471.

(9) Golberg, D.; Bando, Y.; Huang, Y.; Terao, T.; Mitome, M.; Tang, C.; Zhi, C. Boron Nitride Nanotubes and Nanosheets. *ACS Nano* **2010**, *4*, 2979−2993.

(10) Denis, P. A.; Faccio, R.; Mombru, A. W. Is It Possible to Dope Single-Walled Carbon Nanotubes and Graphene with Sulfur? *ChemPhysChem* **2009**, *10*, 715−722.

(11) Xue, Y.; Wu, B.; Jiang, L.; Guo, Y.; Huang, L.; Chen, J.; Tan, J.; Geng, D.; Luo, B.; Hu, W.; Yu, G.; Liu, Y. Low Temperature Growth of Highly Nitrogen-Doped Single Crystal Graphene Arrays by Chemical Vapor Deposition. *J. Am. Chem. Soc.* **2012**, *134*, 11060−11063.

(12) Zheng, B.; Wang, J.; Wang, F.-B.; Xia, X.-H. Synthesis of Nitrogen Doped Graphene with High Electrocatalytic Activity Toward Oxygen Reduction Reaction. *Electrochem. Commun.* **2013**, *28*, 24−26.

(13) Yang, S.; Zhi, L.; Tang, K.; Feng, X.; Maier, J.; Müllen, K. Efficient Synthesis of Heteroatom (N or S)-Doped Graphene Based on Ultrathin Graphene Oxide-Porous Silica Sheets for Oxygen Reduction Reactions. *Adv. Funct. Mater.* **2012**, *22*, 3634−3640.

(14) Higgins, D.; Chen, Z.; Lee, D. U.; Chen, Z. Activated and Nitrogen-Doped Exfoliated Graphene as Air Electrodes for Metal-Air Battery Applications. *J. Mater. Chem. A* **2013**, *1*, 2639−2645.

(15) Chen, P.; Xiao, T.-Y.; Qian, Y.-H.; Li, S.-S.; Yu, S.-H. A Nitrogen-Doped Graphene/Carbon Nanotube Nanocomposite with Synergistically Enhanced Electrochemical Activity. *Adv. Mater.* **2013**, *25*, 3192−3196.

(16) Uchoa, B.; Castro Neto, A. H. Superconducting States of Pure and Doped Graphene. *Phys. Rev. Lett.* **2007**, *98*, 146801−146804.

(17) Cai, D.; Wang, S.; Lian, P.; Zhu, X.; Li, D.; Yang, W.; Wang, H. Superhigh Capacity and Rate Capability of High-Level Nitrogen-Doped Graphene Sheets as Anode Materials for Lithium-Ion Batteries. *Electrochim. Acta* **2013**, *90*, 492−497.

(18) Reddy, A. L. M.; Srivastava, A.; Gowda, S. R.; Gullapalli, H.; Dubey, M.; Ajayan, P. M. Synthesis of Nitrogen-Doped Graphene Films for Lithium Battery Application. *ACS Nano* **2010**, *4*, 6337−6342.

(19) Wang, H.; Zhang, C.; Liu, Z.; Wang, L.; Han, P.; Xu, H.; Zhang, K.; Dong, S.; Yao, J.; Cui, G. Nitrogen-Doped Graphene Nanosheets with Excellent Lithium Storage Properties. *J. Mater. Chem.* **2011**, *21*, 5430−5434.

(20) Some, S.; Kim, J.; Lee, K.; Kulkarni, A.; Yoon, Y.; Lee, S.; Kim, T.; Lee, H. Highly Air-Stable Phosphorus-Doped n-Type Graphene Field-Effect Transistors. *Adv. Mater.* **2012**, *24*, 5481−5486.

(21) Liu, Z.-W.; Peng, F.; Wang, H.-J.; Yu, H.; Zheng, W.-X.; Yang, J. Phosphorus-Doped Graphite Layers with High Electrocatalytic Activity for the O_2 Reduction in an Alkaline Medium. *Angew. Chem., Int. Ed.* **2011**, *50*, 3257−3261.

(22) Yang, D. S.; Bhattacharjya, D.; Inamdar, S.; Park, J.; Yu, J. S. Phosphorus-Doped Ordered Mesoporous Carbons with Different Lengths as Efficient Metal-Free Electrocatalysts for Oxygen Reduction Reaction in Alkaline Media. *J. Am. Chem. Soc.* **2012**, *134*, 16127−16130.

(23) Choi, C. H.; Park, S. H.; Woo, S. I. Phosphorus-Nitrogen Dual Doped Carbon as An Effective Catalyst for Oxygen Reduction Reaction in Acidic Media: Effects of The Amount of P-Doping on The Physical and Electrochemical Properties of Carbon. *J. Mater. Chem.* **2012**, *22*, 12107−12115.

(24) Choi, C. H.; Park, S. H.; Woo, S. I. Binary and Ternary Doping of Nitrogen, Boron, and Phosphorus into Carbon for Enhancing Electrochemical Oxygen Reduction Activity. *ACS Nano* **2012**, *6*, 7084−7091.

(25) Nasini, U. B.; Bairi, V. G.; Ramasahayam, S. K.; Bourdo, S. E.; Viswanathan, T.; Shaikh, A. U. Phosphorous and Nitrogen Dual Heteroatom Doped Mesoporous Carbon Synthesized via Microwave Method for Supercapacitor Application. *J. Power Sources* **2014**, *250*, 257−265.

(26) Wang, C.; Zhou, Y.; Sun, L.; Wan, P.; Zhang, X.; Qiu, J. Sustainable Synthesis of Phosphorus- and Nitrogen-Co-Doped Porous Carbons with Tunable Surface Properties for Supercapacitors. *J. Power Sources* **2013**, *239*, 81−88.

(27) Hulicova-Jurcakova, D.; Puziy, A. M.; Poddubnaya, O. I.; Suárez-García, F.; Tascón, J. M. D.; Lu, G. Q. Highly Stable Performance of Supercapacitors from Phosphorus-Enriched Carbons. *J. Am. Chem. Soc.* **2009**, *131*, 5026−5027.

(28) Cruz-Silva, E.; Cullen, D. A.; Gu, L.; Romo-Herrera, J. M.; Muñoz-Sandoval, E.; López-Urías, F.; Sumpter, B. G.; Meunier, V.; Charlier, J.-C.; Smith, D. J.; Terrones, H.; Terrones, M. Heterodoped Nanotubes: Theory, Synthesis, and Characterization of Phosphorus-Nitrogen Doped Multiwalled Carbon Nanotubes. *ACS Nano* **2008**, *2*, 441−448.
(29) Uthaisar, C.; Barone, V. Edge Effects on the Characteristics of Li Diffusion in Graphene. *Nano Lett.* **2010**, *10*, 2838−2842.
(30) Yan, Y.; Yin, Y.-X.; Xin, S.; Guo, Y.-G.; Wan, L.-J. Ionothermal Synthesis of Sulfur-Doped Porous Carbons Hybridized with Graphene as Superior Anode Materials for Lithium-Ion Batteries. *Chem. Commun.* **2012**, *48*, 10663−10665.
(31) Li, X.; Geng, D.; Zhang, Y.; Meng, X.; Li, R.; Sun, X. Superior Cycle Stability of Nitrogen-Doped Graphene Nanosheets as Anodes for Lithium Ion Batteries. *Electrochem. Commun.* **2011**, *13*, 822−825.
(32) Ning, G.; Fan, Z.; Wang, G.; Gao, J.; Qian, W.; Wei, F. Gram-Scale Synthesis of Nanomesh Graphene with High Surface Area and Its Application in Supercapacitor Electrodes. *Chem. Commun.* **2011**, *47*, 5976−5978.
(33) Zhao, M. Q.; Zhang, Q.; Huang, J. Q.; Tian, G. L.; Nie, J. Q.; Peng, H. J.; Wei, F. Unstacked Double-Layer Templated Graphene for High-Rate Lithium-Sulphur Batteries. *Nat. Commun.* **2014**, *5*, 1−8.
(34) Ning, G.; Xu, C.; Mu, L.; Chen, G.; Wang, G.; Gao, J.; Fan, Z.; Qian, W.; Wei, F. High Capacity Gas Storage in Corrugated Porous Graphene with a Specific Surface Area-Lossless Tightly Stacking Manner. *Chem. Commun.* **2012**, *48*, 6815−6817.
(35) Wei, D.; Liu, Y.; Wang, Y.; Zhang, H.; Huang, L.; Yu, G. Synthesis of N-Doped Graphene by Chemical Vapor Deposition and Its Electrical Properties. *Nano Lett.* **2009**, *9*, 1752−1758.
(36) Li, R.; Wei, Z.; Gou, X.; Xu, W. Phosphorus-Doped Graphene Nanosheets as Efficient Metal-Free Oxygen Reduction Electrocatalysts. *RSC Adv.* **2013**, *3*, 9978−9984.
(37) Claeyssens, F.; Fuge, G. M.; Allan, N. L.; May, P. W.; Ashfold, M. N. R. Phosphorus Carbides: Theory and Experiment. *Dalton Trans* **2004**, *19*, 3085−3092.
(38) Yan, X.; Liu, Y.; Fan, X.; Jia, X.; Yu, Y.; Yang, X. Nitrogen/Phosphorus Co-Doped Nonporous Carbon Nanofibers for High-Performance Supercapacitors. *J. Power Sources* **2014**, *248*, 745−751.
(39) Wang, F.; Yao, G.; Xu, M. W.; Zhao, M. S.; Sun, Z. B.; Song, X. P. Large-Scale Synthesis of Macroporous SnO_2 with/without Carbon and Their Application as Anode Materials for Lithium-Ion Batteries. *J. Alloys Compd.* **2011**, *509*, 5969−5973.
(40) Usachov, D.; Vilkov, O.; Grüneis, A.; Haberer, D.; Fedorov, A.; Adamchuk, V. K.; Preobrajenski, A. B.; Dudin, P.; Barinov, A.; Oehzelt, M.; Laubschat, C.; Vyalikh, D. V. Nitrogen-Doped Graphene: Efficient Growth, Structure, and Electronic Properties. *Nano Lett.* **2011**, *11*, 5401−5407.
(41) Kudin, K. N.; Ozbas, B.; Schniepp, H. C.; Prud'homme, R. K.; Aksay, I. A.; Car, R. Raman Spectra of Graphite Oxide and Functionalized Graphene Sheets. *Nano Lett.* **2008**, *8*, 36−41.
(42) Wei, D.; Liu, Y.; Cao, L.; Fu, L.; Li, X.; Wang, Y.; Yu, G.; Zhu, D. A New Method to Synthesize Complicated Multibranched Carbon Nanotubes with Controlled Architecture and Composition. *Nano Lett.* **2006**, *6*, 186−192.
(43) Ferrari, A. C.; Meyer, J. C.; Scardaci, V.; Casiraghi, C.; Lazzeri, M.; Mauri, F.; Piscanec, S.; Jiang, D.; Novoselov, K. S.; Roth, S.; Geim, A. K. Raman Spectrum of Graphene and Graphene Layers. *Phys. Rev. Lett.* **2006**, *97*, 187401−187404.
(44) Lee, Y. T.; Kim, N. S.; Bae, S. Y.; Park, J.; Yu, S.-C.; Ryu, H.; Lee, H. J. Growth of Vertically Aligned Nitrogen-Doped Carbon Nanotubes: Control of the Nitrogen Content over the Temperature Range 900−1100 °C. *J. Phys. Chem. B* **2003**, *107*, 12958−12963.
(45) Ning, G.; Xu, C.; Zhu, X.; Zhang, R.; Qian, W.; Wei, F.; Fan, Z.; Gao, J. MgO-Catalyzed Growth of N-Doped Wrinkled Carbon Nanotubes. *Carbon* **2013**, *56*, 38−44.
(46) Paraknowitsch, J. P.; Thomas, A. Doping Carbons Beyond Nitrogen: An Overview of Advanced Heteroatom Doped Carbons with Boron, Sulphur and Phosphorus for Energy Applications. *Energy Environ. Sci.* **2013**, *6*, 2839−2855.
(47) Strelko, V. V.; Kuts, V. S.; Thrower, P. A. On the Mechanism of Possible Influence of Heteroatoms of Nitrogen, Boron and Phosphorus in a Carbon Matrix on the Catalytic Activity of Carbons in Electron Transfer Reactions. *Carbon* **2000**, *38*, 1499−1503.
(48) Wang, H.-m.; Wang, H.-x.; Chen, Y.; Liu, Y.-j.; Zhao, J.-x.; Cai, Q.-h.; Wang, X.-z. Phosphorus-Doped Graphene and (8, 0) Carbon Nanotube: Structural, Electronic, Magnetic Properties, and Chemical reactivity. *Appl. Surf. Sci.* **2013**, *273*, 302−309.
(49) Guo, P.; Song, H.; Chen, X. Electrochemical Performance of Graphene Nanosheets as Anode Material for Lithium-Ion Batteries. *Electrochem. Commun.* **2009**, *11*, 1320−1324.
(50) Zhou, H.; Zhu, S.; Hibino, M.; Honma, I.; Ichihara, M. Lithium Storage in Ordered Mesoporous Carbon (CMK-3) with High Reversible Specific Energy Capacity and Good Cycling Performance. *Adv. Mater.* **2003**, *15*, 2107−2111.
(51) Su, D. S.; Schlögl, R. Nanostructured Carbon and Carbon Nanocomposites for Electrochemical Energy Storage Applications. *ChemSusChem* **2010**, *3*, 136−168.
(52) Hassoun, J.; Lee, K. S.; Sun, Y. K.; Scrosati, B. An Advanced Lithium Ion Battery Based on High Performance Electrode Materials. *J. Am. Chem. Soc.* **2011**, *133*, 3139−3143.
(53) Wang, C.; Li, D.; Too, C. O.; Wallace, G. G. Electrochemical Properties of Graphene Paper Electrodes Used in Lithium Batteries. *Chem. Mater.* **2009**, *21*, 2604−2606.
(54) Shin, W. H.; Jeong, H. M.; Kim, B. G.; Kang, J. K.; Choi, J. W. Nitrogen-Doped Multiwall Carbon Nanotubes for Lithium Storage with Extremely High Capacity. *Nano Lett.* **2012**, *12*, 2283−2288.
(55) Lian, P.; Zhu, X.; Liang, S.; Li, Z.; Yang, W.; Wang, H. Large Reversible Capacity of High Quality Graphene Sheets as an Anode Material for Lithium-Ion Batteries. *Electrochim. Acta* **2010**, *55*, 3909−3914.
(56) Hu, J.; Li, H.; Huang, X. Electrochemical Behavior and Microstructure Variation of Hard Carbon Nano-Spherules as Anode Material for Li-Ion Batteries. *Solid State Ionics* **2007**, *178*, 265−271.
(57) Su, Y.; Li, S.; Wu, D.; Zhang, F.; Liang, H.; Gao, P.; Cheng, C.; Feng, X. Two-Dimensional Carbon-Coated Graphene/Metal Oxide Hybrids for Enhanced Lithium Storage. *ACS Nano* **2012**, *6*, 8349−8356.
(58) Oh, S. G.; Rodriguez, N. M. In Situ Electron Microscopy Studies of the Inhibition of Graphite Oxidation by Phosphorus. *J. Mater. Res.* **1993**, *8*, 2879−2888.
(59) Tran, T. D.; Feikert, J. H.; Song, X.; Kinoshita, K. Commercial Carbonaceous Materials as Lithium Intercalation Anodes. *J. Electrochem. Soc.* **1995**, *142*, 3297−3302.
(60) Tang, K.; White, R. J.; Mu, X.; Titirici, M.-M.; van Aken, P. A.; Maier, J. Hollow Carbon Nanospheres with a High Rate Capability for Lithium-Based Batteries. *ChemSusChem* **2012**, *5*, 400−403.